NASA-CR-197752

(NASA-CR-197752) SUPERSONIC TRANSPORT GRID GENERATION, VALIDATION, AND OPTIMIZATION Final Report, 1993 - 31 Jan. 1995 (MCAT Inst.) 15 p

N95-26648

Unclas

G3/61 0048500

MCAT Institute
Final Report
95-03

Supersonic Transport Grid Generation, Validation, and Optimization

Philip G. Aaronson

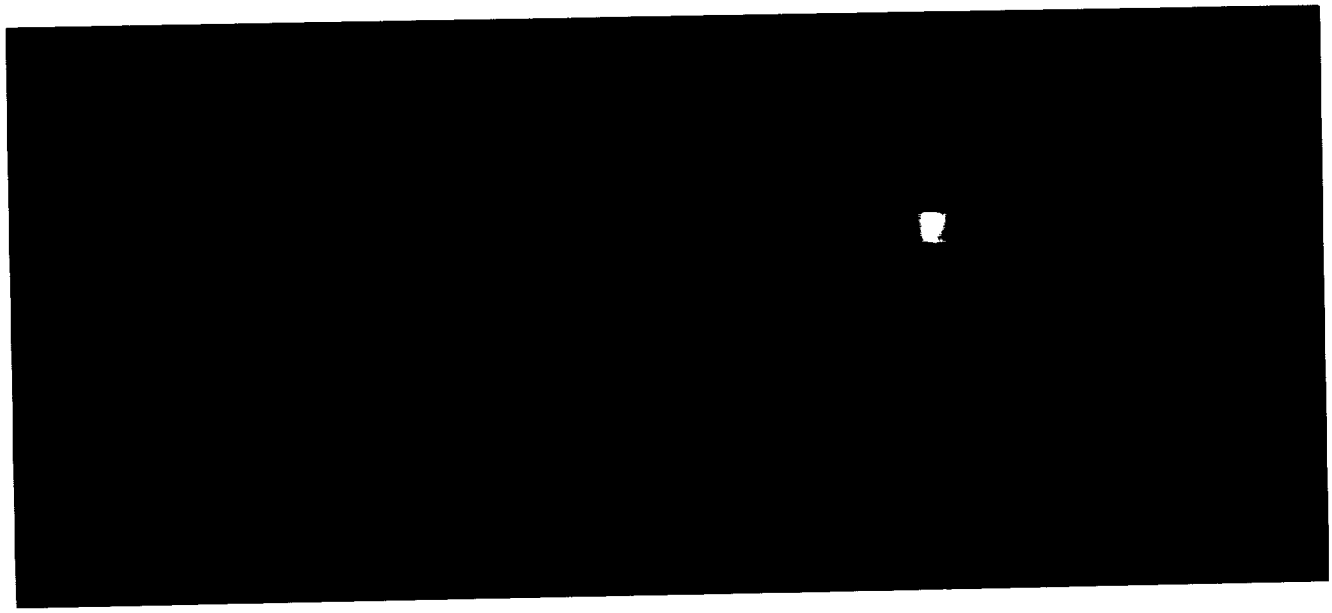

January 1995

NCC 2-522

MCAT Institute
3933 Blue Gum Drive
San Jose, CA 95127

Supersonic Transport Grid Generation, Validation, and Optimization

Philip G. Aaronson

Introduction:

The ever present demand for reduced flight times has renewed interest in High Speed Civil Transports (HSCT). The need for an HSCT becomes especially apparent when the long distance, over-sea, high growth Pacific rim routes are considered. Crucial to any successful HSCT design are minimal environmental impact and economic viability. Vital is the transport's aerodynamic efficiency, ultimately effecting both the environmental impact and the operating cost. Optimization, including numerical optimization, coupled with the use of computational fluid dynamics (CFD) technology, has and will offer a significant improvement beyond traditional methods. Further, a key environmental factor is the sonic boom signature. CFD will play a crucial role in shaping and minimizing the aircraft's sonic boom in order to reduce the perceived loudness that inhabitants experience beneath the flight path.

1993-January 31,1995:

Grid generation has been the focus of this year's efforts. A series of surface grids being generated around a generic nacelle-diverter combination, McDonnell Douglas' Wing 4, and Wing 5 as well as Boeing's Reference H and Configuration 1122.

A generic nacelle-diverter combination mounted on a flat plate was tested in the Langley Research Center Unitary Plan Wind Tunnel in January of 1994 [UPWT Test 1784]. This presented a chance to validate our CFD codes against experimental data and compare results in the difficult nacelle-diverter region. Several sets of grids were generated using ICEMCFD, starting from the mechanical drawings used to fabricate the original wind tunnel model. These included a series of surface grids to be run by Scott Lawrence with his UPS code, as well as a single surface grid and an overset grid set to be run with OVERFLOW.

A series of surface grids on McDonnell Douglas' Wing 4 and Wing 5 geometry was generated using ICEMCFD. A two zone topology which I designed was selected as the best means of gridding up the wing-body geometry for the UPS code. This approach minimizes the number of grid points crossing the wing/fuselage juncture.

IGES files obtained from McDonnell Douglas defined the geometry. Wing 4 and Wing 5 was then run by Scott Lawrence using the UPS and Stuff codes. See Fig. 1

Reference H has been an ongoing project with Steve Ryan and myself. A further refined single nacelle, Euler test case was completed. This included the newly defined aft end of the diverter which was obtained from Boeing. Results of the Euler analysis were published as, Philip G. Aaronson and James S. Ryan, "OVERFLOW Code Validation Study for the Boeing Reference H," Proceedings of the First NASA/Industry High Speed Research Propulsion/Airframe Integration Workshop, Cleveland, OH, October 26-27, 1993. A copy of the paper is not included in the appendix due to the competitively sensitive nature of the material. Continued work with the Reference H has resulted in several versions of a complete Navier-Stokes grid about the entire geometry. This includes both nacelles and diverters.

Two versions of a grid about the Boeing configuration 1122 were completed for Samson Cheung. The 1122 configuration proved an especially challenging geometry to create a grid on due to the low wing nature of the aircraft. The wing in places, essentially defined the lower surface of the fuselage making the intersection between the fuselage and wing difficult to accurately capture. See Fig. 2.

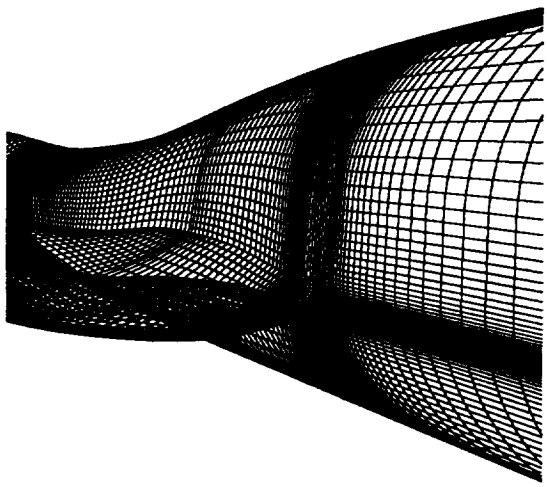

Figure 1. Wing 4 geometry detailing the wing-fuselage juncture.

1992-1993:

Optimization of the Haack-Adams body was the highlight of the research efforts during this one year period. In addition training on the CAD and grid generation system ICEMCFD was completed. Using ICEM, grids were generated about the Boeing 1807 and Model3 geometries.

The Haack-Adams body is a classic linear theory, minimum drag shape. This we used as the initial condition for the optimizer NPSOL in conjunction with the flow solvers UPS and OVERFLOW. An extension of the Fourier series which linear theory analytically defined the Haack-Adams body was used to perturb the shape. The objective function used in this case was the drag of the body. With NPSOL, approximately a 4% reduction in drag was obtained using both Euler and Navier-Stokes flow solutions to determine the objective function. Factors effecting the optimization process such as number of design variables, Mach number, constraints, etc. were extensively discussed. A copy of the paper which has been published by The Journal of Aircraft, Vol.32, January-February 1995 is included in Appendix A.

1991-1992:

This period of research was focused primarily with familiarization with CNS, NPSOL and the other CFD, and optimization tools available at Ames. To achieve that end I ran a series of test problems, a flat plate, wedge, and symmetrical wing.

The flat plate problem was the first project completed upon entering Ames and thus it served the double purpose of familiarizing myself with CNS and running needed test cases against which newly developed codes could be benchmarked. A copy of the technical note which was distributed throughout the group can be found in the '92 annual report and it details all of the initial work completed on the flat plate problem. Further, turbulent flat plate cases were run for comparisons with the then newly developed parallel OVERFLOW code.

The wedge problem was an attempt to model one of the experiments by Holden and Moselle and to compare against UPS's solution to the same problem. Unfortunately UPS never achieved a good agreement with the experimental data, and the solutions run by CNS (F3D) had an even worse agreement.

Within the laminar flow control group, Joseph Garcia is doing a study on the transition location for various planform shapes. Laminar viscous solutions were needed around each planform in order to then generate the transition location. This

planform was exactly what was needed for testing of new boundary conditions in CNS and as a test case for a CNS/NPSOL optimizer combination.

Figure 2. Boeing Configuration 1122 grid showing detail of the wing-fuselage juncture.

Appendix A

NLE

CFD OPTIMIZATION OF A THEORETICAL MINIMUM-DRAG BODY

Samson Cheung* and Philip Aaronson**
MCAT Institute
Moffett Field, California

Thomas Edwards†
NASA Ames Research Center
Moffett Field, California

Abstract

The increasing performance and environmental demands required of an aircraft necessitates the development of a set of design tools capable of meeting these challenges. This paper describes a methodology behind coupling a fast, parabolized Navier-Stokes flow solver to a nonlinear constraint optimizer. The design parameters, constraints, grid refinement, behavior of the optimizer, and flow physics related to the CFD calculations are discussed. A theoretical minimum-drag body of revolution is chosen as an initial configuration for the optimization process. For the slender axisymmetric body, a calculation including nonlinear and viscous effects produces a different minimum drag geometry than linear theory and results in a drag reduction of approximately 4%. This design tool can be used in aerodynamic optimization and sonic boom minimization of supersonic aircraft. The High Speed Civil Transport is a prime example.

Introduction

The need for computational fluid dynamics (CFD) in aerodynamic optimization is highlighted as the supercomputer plays an increasing role in aerodynamic research. One of NASA's research thrusts, the High Speed Research Program (HSRP), defines challenges in sonic boom, and aerodynamic optimization. The primary focus is the High Speed Civil Transport (HSCT),[1] which is the next generation supersonic passenger aircraft. In this paper, the techniques and tools of aerodynamic optimization will be described. A theoretical minimum drag body of revolution is chosen as the baseline configuration for the optimization process.

A shape perturbation method is chosen for optimization in the present study. A similar method was used extensively by Haney, Johnson, and Hicks[2] to optimize transonic wings. In their method a potential flow solver was coupled with a feasible direction algorithm. The design variables were the scalar coefficients of a finite set of chosen sine and exponential functions. These functions were then added to the upper surface of the wing, perturbing the wing's shape. Cosentino and Holst[3] coupled the TWING and QNM codes and performed a spline fit across control points located on the upper surface of the wing. In a two-dimensional analysis, Vanderplaats and Hicks[4] coupled a potential code with the constraint optimizer CONMIN. Polynomial coefficients were used as design functions; lift and wave drag were used as test case objective functions. Aero-function shapes were developed through the use of an inverse optimization process by Aidala, Davis, and Mason.[5] These were used with a potential flow code coupled to CONMIN. Each shape was designed to control an aspect of the pressure distribution and then employed as a design variable in the optimization process. The present method takes advantage of a Fourier sine series that defines the original body. The Fourier coefficients are convenient, physically relevant design variables.

As a test case, the Haack-Adams[6,7,8] (H-A) theoretical minimum drag body of revolution is chosen. The H-A body is selected in this study because it is a classic aerodynamics problem for which validating experimental data[9] are available. Because of its simple geometry, running large numbers of permutations is still relatively inexpensive. And since the geometry ends in a finite base, it is particularly well suited for space-marching codes. By including viscous and other nonlinear effects it is hoped that a new optimum may be located.

In the following sections the H-A body is first derived and then the CFD flow solver is validated

* Research Scientist, Member AIAA.
** Junior Research Scientist.
† Assistant Chief, Computational Aerosciences Branch. Senior Member AIAA.

on the geometry over a range of Mach numbers and grid densities. Then the optimization procedure is described, including optimizer behavior, design variable studies, and the constraints used. Finally, several runs of the optimizer/flow solver are completed on the H-A body and the results are presented.

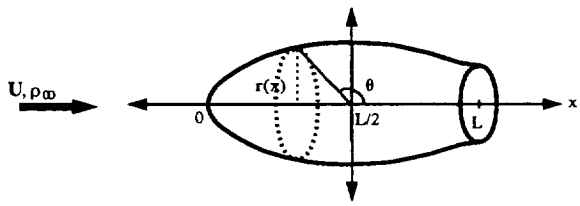

Figure 1. A body of revolution.

Haack-Adams Body

The H-A body is a classic aerodynamic shape derived from supersonic slender body theory. This shape minimizes the wave drag subject to constraints on the volume and base area. The H-A body was chosen as an optimization test case for its database of experimental data which can be used to verify the CFD code. The simplicity of the geometry makes grid generation relatively easy and robust. The finite base of the H-A body facilitates correlation with an experimental models which have an attached sting, and simplifies modeling with space-marching codes.

Slender-body theory, which was used in deriving the H-A body shapes, is a special case of small perturbation potential-flow theory with the additional restriction that the product $r\sqrt{M_\infty - 1}$ is much smaller than x, where r is radius of the body at some streamwise distance x along the axis of the body, and M_∞ is the freestream Mach number. The theory described in this section can be found in most aerodynamic textbooks,[10,11] but is reviewed here for convenience.

Consider supersonic flow of velocity U and density ρ_∞ over a body of revolution of length L as shown in Fig. 1. The velocity potential due to a linear source distribution of strength $Uf(x)$ is

$$\phi(x) = -\frac{1}{2\pi}\int_0^{x-\beta r} \frac{f(\xi)}{(x-\xi)^2 - \beta^2 r^2}\, d\xi$$

where $\beta = \sqrt{M_\infty - 1}$ and $x = L(1+\cos\theta)/2$. Expressing f as a Fourier sine series,

$$f(\theta) = L\sum_{n=1}^{\infty} \alpha_n \sin(n\theta)$$

The derivative of the cross-sectional area, A', can be approximated by f. Integrating f produces,

$$A(\theta) = \int_\pi^\theta f(\theta)\, d\theta$$

$$= -\frac{L^2}{2}\int_\pi^\theta \sum_{n=1}^{\infty} [\alpha_n \sin(n\theta)][\sin\theta]\, d\theta$$

$$A(\theta) = \frac{L^2}{4}\left\{\alpha_1(\pi - \theta + \frac{1}{2}\sin 2\theta) + \alpha_2\frac{4}{3}\sin^3\theta + \sum_{n=3}^{\infty}\alpha_n\left(\frac{\sin(n-1)\theta}{n-1} - \frac{\sin(n+1)\theta}{n+1}\right)\right\} \quad (1)$$

Slender-body theory gives the formula of wave drag,

$$D_w = \frac{\pi\rho_\infty U^2 L^2}{8}\sum_{n=1}^{\infty} n\alpha_n^2 \quad (2)$$

Equations (1) and (2) show that the cross-sectional area and the wave drag are independent of the Mach number. The H-A body is defined by the body shape that minimizes D_w subject to the following conditions:

C1 ≡ the area at the base $A(L) = A_{base}$ is fixed and non-zero
C2 ≡ the slope of the body is zero at the base, $\left(\frac{dA}{dx}\right)\Big|_{x=L} = 0$
C3 ≡ the finess ratio is fixed.

It is easy to check that Eq. (1) satisfies C2. The remaining two conditions C1 and C3 determine the values of α_1 and α_2. In order for a body to produce minimum drag, Eq. (2) suggests that $\alpha_n = 0$ for $n \geq 3$. Condition C1 gives

$$\alpha_1 = \frac{4A_{base}}{L^2\pi} \quad (3)$$

and C3 gives x_{max}, the location of the maximum thickness, and therefore,

$$\alpha_2 = \frac{\alpha_1}{2\cos\theta_{max}}, \quad \theta_{max} = \cos^{-1}\left(\frac{2x_{max}}{L} - 1\right) \quad (4)$$

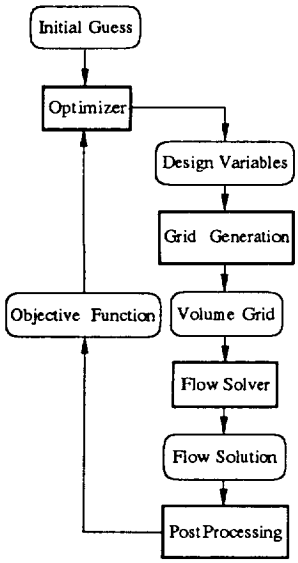

Figure 2. Diagram of optimization procedure.

Optimization Procedure

The optimizer first generates a baseline objective function from the initial values of the design variables supplied as input. The optimizer then perturbs each of the design variables in order to locate a search direction. During each perturbation, a surface grid and computational grid are generated. The flow is then solved on the computational grid and from this, the objective function is produced. The optimizer continues to perturb and search until a set of design variables, and thus a new body shape, is obtained with a local minimum objective function (see Fig. 2). Both linear and nonlinear constraints can be added to the design variables.

Design Variables

Perturbations are performed through the use of design variables that have a direct influence on the objective function. The design variables used here were inspired by the original Fourier sine series used in the derivation of the H-A body. Equation (1) can be rewritten using Eqs. (3) and (4) as

$$\frac{r^2}{r_{max}^2} = \frac{A_{base}}{\pi A_{max}}\left\{(\pi - \theta + \frac{1}{2}\sin 2\theta) + \gamma_1 \frac{4}{3}\sin^3\theta + \sum_{m=2}^{\infty}\gamma_m\left(\frac{\sin(m)\theta}{m} - \frac{\sin(m+2)\theta}{m+2}\right)\right\} \quad (5)$$

where $\gamma_m = \alpha_m/\alpha_1$ for $m = 2, 3, ..., \infty$. r_{max} and A_{base}/A_{max} are known. According to linear theory, the γ_m are set to zero. However, since nonlinear effects are included in the CFD analysis, a finite number of these coefficients ($m = 2, 3, ..., N$) were chosen as the design variables. Therefore, the optimized configuration will also be defined by Eq. (5).

Constraints

It is important to check that this optimal configuration satisfies the three conditions (C1, C2, and C3) of the H-A body. Equation (5) satisfies C1 when evaluated at $\theta = 0$ and $(dA/dx = \pi d(r^2)/dx)$.

$$\frac{dA}{d\theta}\frac{d\theta}{dx} = -\frac{2A_{base}}{L\ A_{max}}\left\{-\frac{2\sin^2\theta}{\sin\theta} + \gamma_1\frac{4\sin^2\theta\cos\theta}{\sin\theta} + \sum_{m=2}^{N}\gamma_m\left(\frac{\cos(m)\theta - \cos(m+2)\theta}{\sin\theta}\right)\right\} \quad (6)$$

Equation (6) is zero when evaluated at $\theta = 0$. Note that the terms inside the summation sign are zero by L'Hôpital's Rule, thus, C2 is satisfied. Slender-body theory and condition C3 requires the H-A body to satisfy $(dA/dx)|_{x=x_{max}} = 0$. In the optimization process, the location of the maximum was allowed to change in such a way that $-1 \leq (dA/dx)|_{x=x_{max}} \leq 1$, that is

$$\left|-2\sin^2\theta_{max} + 4\gamma_1\sin^2\theta_{max}\cos\theta_{max} + \sum_{m=2}^{N}\gamma_m\left(\cos(m)\theta_{max} - \cos(m+2)\theta_{max}\right)\right| \leq 1 \quad (7)$$

This constraint limits the amount x_{max} (or θ_{max}) could shift in order to prevent excessive skewness in the grid. On the original H-A body x_{max} was fixed. An additional requirement is needed to ensure that the radius of the optimal body (Eq. 5) is always greater than or equal to zero; that is,

$$(\pi - \theta + \frac{1}{2}\sin 2\theta) + \gamma_1\frac{4}{3}\sin^3\theta + \sum_{m=2}^{N}\gamma_m\left(\frac{\sin(m)\theta}{m} - \frac{\sin(m+2)\theta}{m+2}\right) \geq 0 \quad (8)$$

for all $0 \geq \theta \geq \pi$. Equations (7) and (8) set the relationships among the γ's and are treated as constraints for the optimization problem. It should be noted that due to the Fourier nature of the shape functions, the volume of the optimal body (Eq. 5) is the same as that of the original H-A body.

Flow Solver

The implemented CFD flow solver is the 3-D parabolized Navier-Stokes code, UPS3D.[12] This is a space-marching code that calculates steady-state viscous or inviscid solutions to supersonic flows. A conic

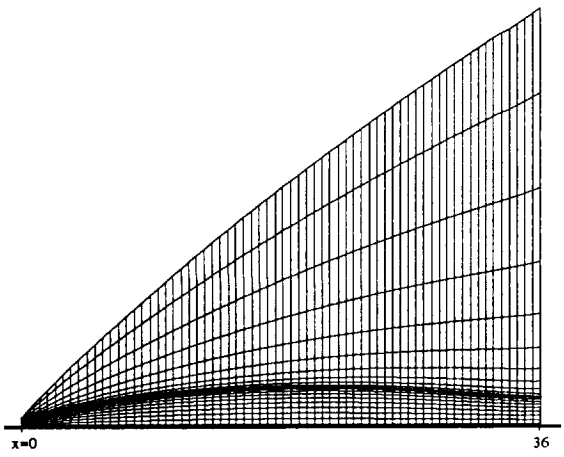

Figure 3. Schematic marching grid of of the Haack-Adams body.

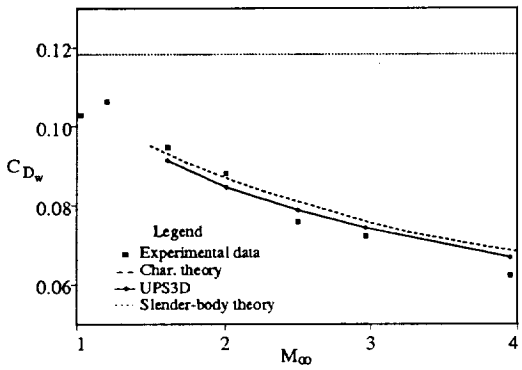

Figure 4. Wave drag comparison over a range of Mach numbers, $\frac{L}{2R_{max}} = 7$.

approximation is made for the initial marching plane. This code is further supported by a hyperbolic grid generation scheme[13] that is sufficiently fast and robust to operate within an automated optimization environment. In this study, both viscous and inviscid supersonic calculations are employed. From these solutions, the drag coefficient C_D is calculated by integrating pressure and skin friction (if applicable) over the surface of the body. The UPS3D code uses a step size of 0.1% of the body length (L) on a grid of 21 points in the circumferential direction and 50 points in the body-normal direction. The grid points are clustered near the body surface (see Fig. 3).

Objective Function

Five design variables, namely, $\gamma_2, \gamma_3, \ldots, \gamma_6$ of Eq. (5) are used in the majority of the remainder of this study. At each step, the optimizer alters the γ values and a new shape is defined. A new computational grid is then created and UPS3D calculates the flow over this new geometry. The wave drag coefficient (C_{Dw}) is determined by numerical integration of the pressure coefficient (C_p) over the body

$$C_{Dw} = \iint \frac{C_p}{A_{max}} dS(x) = \int_0^x \frac{2\pi r C_p}{A_{max}} \left(\frac{dr}{dx}\right) dx$$

If skin friction as well as pressure is included in the integration then total drag is calculated.

Optimizer

The optimizer, NPSOL,[14] is a collection of Fortran subroutines designed to solve the nonlinear programming problem:

$$\text{minimize } F(x)$$

$$\text{subject to : } l \leq \begin{bmatrix} x \\ Ax \\ c(x) \end{bmatrix} \leq u$$

where $F(x)$ is the objective function, x is a vector of length n that contains the design variables, $c(x)$ contains the nonlinear constraint functions, and A is the linear constraint matrix. Note that u and l, the upper and lower bounds, are vectors and thus are specified for each variable and constraint.

NPSOL uses a sequential quadratic programming algorithm to look for the minimum of $F(x)$. Within each iteration, the search direction is the solution of a quadratic programming (QP) algorithm. Each QP subproblem is solved by a quasi-Newton approximation. The optimizer stops when it finds a local minimum of $F(x)$.

The user needs to define $F(x)$, A, $c(x)$ and the bounds for each, as well as an initial estimate of the solution. An important consideration is the difference interval used in the finite difference approximation of the gradient. NPSOL has an option to calculate the difference interval; however, this involves a large number of calls to the flow solver, which is impractical. The difference interval is specified as an input throughout this study.

Results and Discussion

Test Cases

Flow Solver As a validation test case, the UPS3D code run in inviscid mode is compared against the experimental data. A review of Fig. 3 illustrates a typical grid used by UPS3D, which shows the surface as well as a plane normal to the body. In the experimental study,[9] the H-A body had a length L of 36" with a fineness ratio $L/2r_{max}$ of 7. The location of maximum thickness was $x_{max} = 21$" ($\theta_{max} = \cos^{-1}(\frac{1}{6})$), and $A_{base}/A_{max} = 0.532$.

The UPS3D code was tested over a range of supersonic Mach numbers and compares well with characteristic theory and experimental data (see Fig. 4).

Note the variation of wave drag with Mach number predicted by both the characteristic theory and inviscid CFD solutions. Slender body theory predicts no variation of drag with Mach number (see Eq. 2).

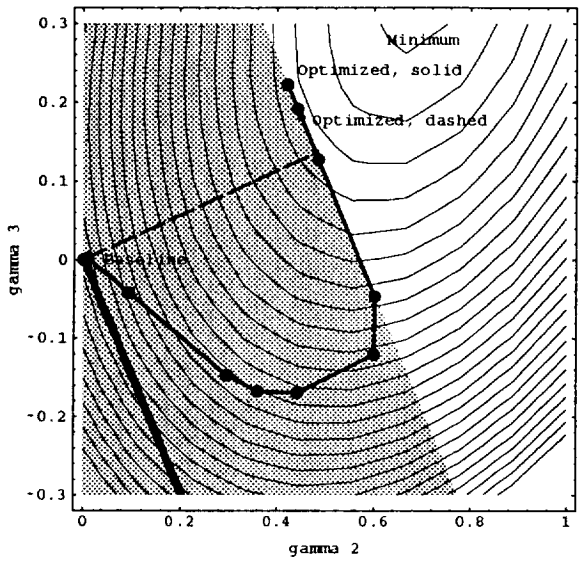

Figure 5. Constrained optimization paths for a difference interval of $\Delta\gamma = 0.01$ (solid line) and $\Delta\gamma = 0.005$ (dashed line).

Optimizer As a test case for the optimizer, NPSOL was run using the analytic slender-body formula for drag (Eq. 2) as the objective function. For this test case, the $\alpha_n, (n = 1, 2, ..., 5)$ coefficients were the design variables and the constraints C1 through C3 were implemented. The design variables were set to arbitrary non-zero values. Within six iterations the optimizer minimized C_{D_w} by locating α_1 and α_2 at the slender-body predicted values, and setting α_3 through α_5 to zero.

In order to visualize the process of optimization, a two-design-variable (γ_2 and γ_3) case is considered. Figure 5 is a contour plot of the wave drag coefficient with respect to γ_2 and γ_3. The dots in the figure are iterative points in the optimization. Linked together, they form a search path. The thickest solid line satisfies the equation $(dA/dx)|_{x=x_{max}} = 0$, and the shaded area satisfies the inequality $-1 \leq (dA/dx)|_{x=x_{max}} \leq 1$, (Eq. (7)), which is the constraint used. The thinner solid line and the dashed line are search paths used by NPSOL with difference intervals of $\Delta\gamma = 0.01$ and $\Delta\gamma = 0.005$, respectively. The larger difference interval calculates a less accurate gradient and thus locates a minimum more slowly than the smaller difference interval. However, there are two local minima in this design space along the constraint boundary. The larger difference interval found the better of the two minima. The smaller difference interval stopped before it found that minimum. This is not always the case, as a larger difference interval could miss a local minimum by "stepping" over it entirely.

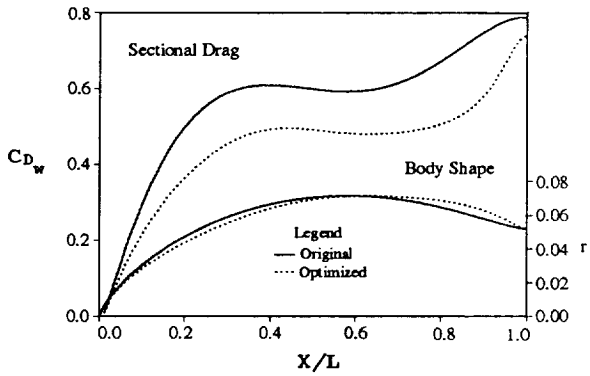

Figure 6. Inviscid optimization with five design variables. $M_\infty = 2.5$, $\frac{L}{2R_{max}} = 7$.

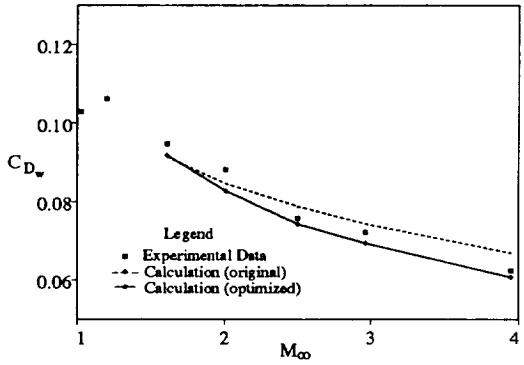

Figure 7. Wave drag comparison between the original H-A body and the H-A body optimized at $M_\infty = 2.5$, over a range of Mach numbers, $\frac{L}{2R_{max}} = 7$.

Inviscid Optimization

The inviscid optimization process gave the result shown in Fig. 6 for a freestream Mach number of 2.5 and an angle of attack of zero degrees. The sectional wave drag coefficient is plotted along with the radius of the original and optimized shapes. During optimization the volume of the forebody is reduced in order to improve the sectional wave drag in this region. The improvement over the original H-A body is reduced aft of the maximum cross-sectional area because of an increase in volume that occurred satisfying the constraints (C1 and C2). Overall, the wave drag of the Haack-Adams body was reduced by 5%. Although the optimized body was designed at Mach 2.5, Fig. 7 shows that the same optimized

body gives lower drag than the H-A body at other Mach numbers. Using $\Delta\gamma = 0.01$, 48 new body shapes were generated and analyzed to reach this result. The whole process took approximately 2.5 CPU hours on the Cray-YMP. Each flow solution calculated by UPS3D uses 160 sec., with an additional 1.3 sec. in grid generation.

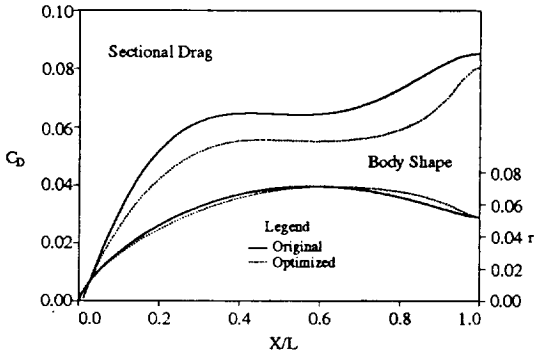

Figure 8. Navier-Stokes optimization with five design variables, $M_\infty = 2.5$, $\frac{L}{2R_{max}} = 7$, $Re = 9 \times 10^6$.

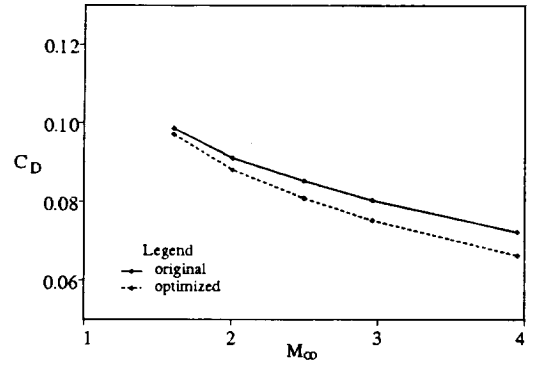

Figure 9. Total drag comparison between the original H-A body and the H-A body optimized with 5 design variables at $M_\infty = 2.5$, over a range of Mach numbers, $\frac{L}{2R_{max}} = 7, Re = 9 \times 10^6$.

Viscous Optimization

The same design procedure was also performed with viscosity taken into account. The result is shown in Fig. 8. The optimizer took much the same strategy as the inviscid case in that the nose of the body was reduced, while a penalty was paid at the rear of the body. The viscous drag results include both wave and skin friction drag, so while the actual drag reduction is comparable to the inviscid optimization, the improvement in this case is 4%. Figure 9 shows that the same body gives lower drag than the original at other Mach numbers. This optimization process with $\Delta\gamma = 0.01$ took about 3.5 CPU hours total on the Cray-YMP and employed 40 flow solutions. Each solution took UPS3D 320 sec with an additional 1.3 sec utilized in grid generation. Table 1 gives the values of the design variables for the inviscid and viscous optimization processes.

Haack-Adams Body $M\infty = 2.5$					
	γ_2	γ_3	γ_4	γ_5	γ_6
Inviscid	0.853	0.673	0.495	0.420	0.0846
Viscous	0.679	0.598	0.353	0.264	0.01875

Table 1. Optimized γ values.

Off-Design Performance

The effects of off-design angle of attack and Reynolds number on the performance of the new, optimized shape were also investigated. For the body that was optimized at zero degree angle of attack, the effects of nonzero angles of attack are shown in Fig. 10. As α increases, the reduction of drag versus the original decreases slightly.

The lower half of Fig. 11 indicates the radial distribution results of three optimization processes at differing Reynolds numbers. The solid line is the original H-A body, the dashed line is the body optimized at a Reynolds number of 10^6, and the dotted line is the body optimized at a Reynolds number of 10^5. The sectional total drag coefficient of these three configurations calculated at a Reynolds number of

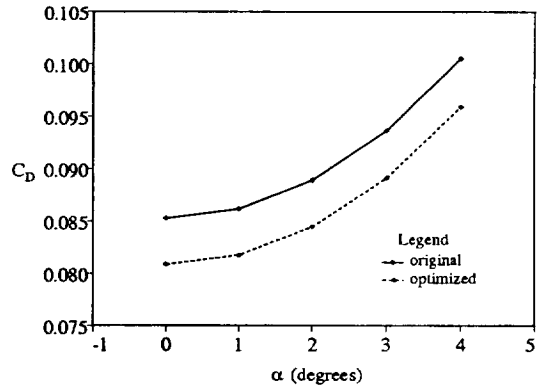

Figure 10. Total drag comparison between the original H-A body and the H-A body optimized with 5 design variables at $M_\infty = 2.5$ and $\alpha = 0$, over a range of α, $\frac{L}{2R_{max}} = 7$, $Re = 9 \times 10^6$.

10^6 is shown in the upper half of the figure. The lower Reynolds number case, which features thicker boundary layers, and hence greater flow displacement, shows the largest perturbation in geometry from the H-A body.

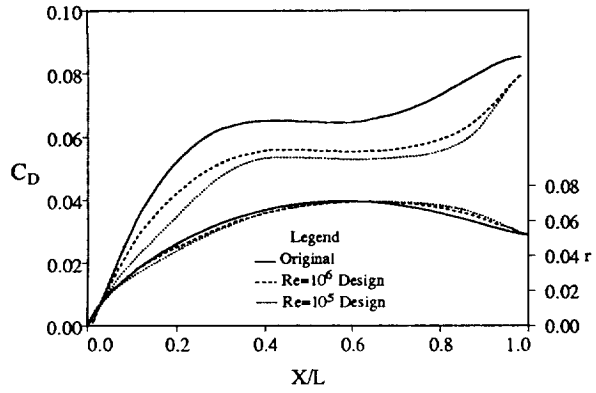

Figure 11. Total drag comparison between the original and optimized H-A bodies with five design variables at $M_\infty = 2.5$ and $\alpha = 0$, for Re= 10^6, and Re= 10^5, computed at Re= 10^6, $\frac{L}{2R_{max}} = 7$.

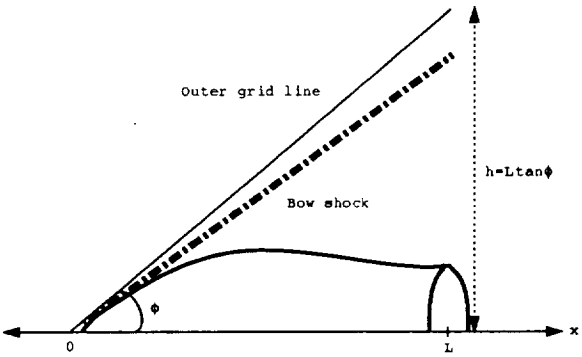

Figure 12. Relationship between the size of the computational grid and the bow shock.

Grid Refinement

A calculation performed on a coarse grid will, in general, contain a larger numerical error than one performed on a fine grid. However, the coarser grid will, in most cases, run significantly faster. It is desirable to reduce the computer time by using the coarsest grid possible that will still yield a physically accurate result. The key to running an optimizer/flow solver efficiently is to choose a sufficiently coarse grid that the cumulative CPU time does not become excessive, yet a fine enough grid to locate a physically valid optimum.

In this grid-refinement study, an optimization problem at Mach 2.5 and zero-degree angle of attack was considered. The computational grid had 21 points in the circumferential direction and the step size of the UPS3D code was taken to be 0.1% of the body length. The grid resolution in the circumferential direction and the step size were fine enough to be kept fixed; only the number of grid points (P) in the normal direction was altered. The distance between the first grid point (in the normal direction) and the surface grid is less than or equal to $s = 0.5(h/P)$, where h, given by $L\ \tan(\phi)$, is the vertical distance from the end of the body to the outer grid (see Fig. 12). Due to grid effects, the calculated bow shock position of the H-A body differed with grid density until the grid was dense enough to resolve the physical shock location. For each computational grid, the angle ϕ was chosen so that the bow shock was as close as possible to the outer boundary. Table 2 gives the values of ϕ and s with different computational grids.

Grid Points (P)	ϕ (degree)	**Spacing** (s/L)
10	50	0.060
20	42	0.025
30	38	0.013
40	36	0.009
50	32	0.006
60	31	0.005
70	30	0.004
95	30	0.003

Table 2. Normal grid points vs. shock location.

The behavior of the flow solution and optimization results on the various grids are analyzed to characterize the errors arising from grid density. For clarification, the following definitions are introduced:

$D(P) \equiv$ C_D calculated on a P-point H-A grid.

$D(\infty) \equiv$ C_D calculated on an asymptotic H-A grid (approximated by 95 points).

$D^m(P) \equiv$ C_D calculated on a P-point grid whose surface shape is obtained in an optimization process on an m-point grid.

$\Delta D^P(P) \equiv |D^P(P) - D^\infty(\infty)|$ the approximate drag reduction of a new design which was obtained by the optimization process on a P-point grid.

$\Delta D^P(\infty) \equiv |D^P(\infty) - D^\infty(\infty)|$ the actual drag reduction of the new design which was obtained by the optimization process on a P-point grid.

The errors due to grid density in the CFD computations of the H-A body and the optimized design are given by $|D(P) - D(\infty)|$ and $|D^P(P) - D^P(\infty)|$, respectively. Both curves are plotted in Fig. 13 and show a roughly exponential decay in error due to grid density. Fig. 14 reveals the grid effect in the optimization process and the CFD calculations. The dashed curve is the error due to grid density in the optimization process, given by $\Delta D^P(P)$. The solid curve is the error due to grid density in optimization and the CFD calculation, given by $\Delta D^P(\infty)$. This figure indicates that the optimization process does not require an overly fine grid in order to locate a physical optimum.

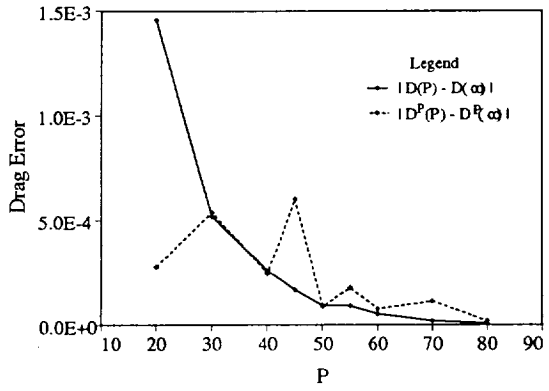

Figure 13. Comparison of the error due to grid density (normal direction) of the original body vs. the modified body. The modified body has been optimized at each of the normal point grids.

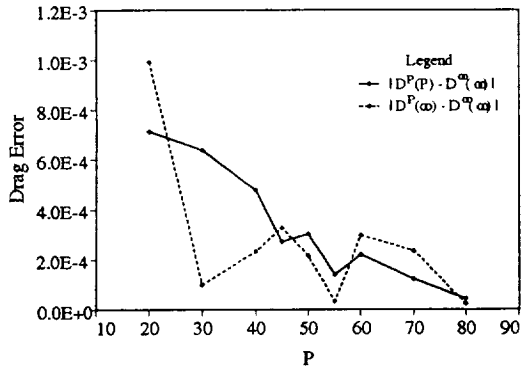

Figure 14. The effects of the number of grid points in the normal direction on the optimization process.

The grid used in the optimization process still has to be fine enough to capture the flow properties and relevant physics in order to obtain a grid-independent optimum. For example, if the grid with $P = 30$ is used, the computed bow-shock is too far away from the exact location, and thus the optimized result has an understandably large error. If the grid with $P = 50$ is used, the flow physics is much more realistically approximated, and the optimized result has a much smaller error (compare the error at $L = 50$ in Fig. 14).

Design Variables

As the number of design variables increases, so do the degrees of freedom of the optimization process. Often the larger the number of design variables in the optimization process, the larger the reduction in drag. Figure 15 displays the optimized C_{D_w}, from inviscid flow solutions with $M_\infty = 2.5$ under different numbers of design variables. Each square in the figure represents the drag coefficient obtained from the optimization process with an initial guess of $\gamma_i = 0$, $i = 1...N$. Thus as a baseline, the original H-A body is employed. Each diamond represents an initial guess of $\gamma_i = 0.1$, $i = 1...N$. For the cases with three and six design variables, the optimized C_{D_w} does not quite follow the expected reduction in C_{D_w}. This is due to a local minimum around the baseline H-A body for those sets of design variables. By adjusting the initial guess the expected result is obtained.

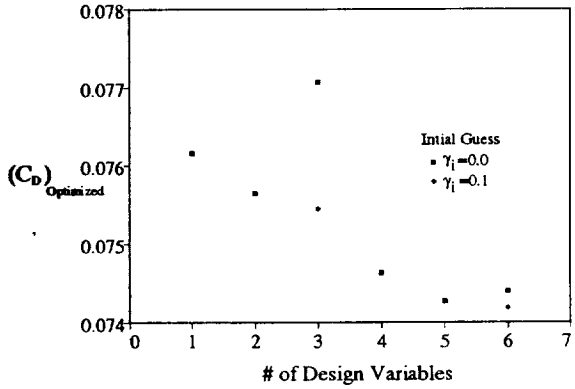

Figure 15. The effects of number of design variables and their initial values on the optimized wave drag. $M_\infty = 2.5$, $\frac{L}{2R_{max}} = 7$.

Conclusions

An aerodynamic optimization procedure has been developed that uses CFD to evaluate aerodynamic performance metrics, and numerical optimization to

develop improved designs. The present implementation uses a parabolized Navier-Stokes solver for aerodynamic analysis of viscous or inviscid supersonic flows. Design variables and objective functions are user-specified, and the optimization process is fully automated.

To validate and evaluate the new capability, a minimum-drag body of revolution was used as a test case. The flow solver was first validated with experimental data and analytical results for the baseline configuration. Then, a series of optimization problems were performed that tested the accuracy and efficiency of the process. When slender body theory is used for the aerodynamic analysis, the optimizer produces a design identical to the theoretical minimum-drag shape. However, using the Euler or Navier-Stokes equations to model the flow produces a slightly different design that has up to 5% lower drag than the original minimum-drag body. Although the test configuration was simple, the results demonstrate the opportunity for significant drag reduction on more complex configurations as well, such as wing-bodies. Equally important, the drag improvement seen at the design condition was demonstrated at off-design conditions.

Using CFD for aerodynamic optimization is a computationally expensive option. This expense can be partially offset by using coarse grids, as long as the errors associated with grid resolution do not invalidate the flow solution. In this study, it was found that valid optimization results could be obtained using grids with about half as many points as were required for grid-independent flow solutions. The interrelation of the optimizer and the flow solver is dependent on the design variables, objective functions and physical flow features, though, so this observation may not be general to other optimization problems.

The selection of design variables has a large impact on the computational expense of the optimization problem as well. The design variables map out the design space in which the optimizer operates. For rapid, robust optimization, this space should define an easily identifiable minimum in the objective function. In this case, the Fourier series coefficients provided a compact definition of the design that clearly demonstrated this attribute.

In summary, the results have shown that aerodynamic optimization using CFD is a practical technology for well posed, moderately sized problems. This capability is currently being applied to the design of supersonic aircraft configurations. The modularity of this approach makes it straightforward to include other disciplines in the optimization process as well, such as structural deformations and propulsion system effects.

References

1. First Annual High-Speed Research Workshop, NASA CP-10087, Part 1, Williamsburg, Virgina, May 14-16, 1991.
2. Haney, H. P., Johnson, R. R., and Hicks, R. M., "Computational Optimization and Wind Tunnel Test of Transonic Wing Designs," AIAA paper 79-0080, Jan., 1979.
3. Cosentino, G. B. and Holst, T. L., "Numerical Optimization Design of Advanced Transonic Wing Configurations," NASA TM 85950, May 1984.
4. Vanderplaats, G. N., and Hicks, R. M., "Numerical Airfoil Optimization Using a Reduced Number of Design Coordinates," NASA TM X-73,151, July 1976.
5. Aidala, P. V., Davis, W. H. Jr., and Mason, W. H., "Smart Optimization," AIAA paper 83-1863, July 1983.
6. Adams, A. C., "Determination of Shapes of Boattail Bodies of Revolution for Minimum Wave Drag," NACA TN-2550, 1951.
7. Haack, W., "Projectile Shapes for Smallest Wave Drag," Translation No. A9-T-3, Contract W33-038-ac-15004 (16351), ATI No. 27736, Air Force Materiel Command, U.S. Air Force, Brown Univ., 1948.
8. Sears, W. R., "On Projectiles with Minimum Wave Drag," Quart. Appl. Math., vol. IV, no. 4, Jan., 1974, pp. 361-366.
9. Harris, R. and Landrum, E., "Drag Characteristic of a Series of Low-Drag Bodies of Revolution at Mach Numbers from 0.6 to 4.0," NASA TN D-3163, Dec., 1965.
10. Ashley, H. and Landahl, M., *Aerodynamics of Wings and Bodies*, Addision-Wesley, 1965.
11. Sears, W., *General Theory of High Speed Aerodynamics - Part C: Small Perturbation Theory*, High Speed Aerodynamics and Jet Propulsion, Vol. VI, Princeton University Press, 1954.
12. Lawrence, S., Chaussee, D., and Tannehill, J., "Application of an Upwind Algorithm to the 3-D Parabolized Navier-Stokes Equations," AIAA paper, 87-1112, June 1987.
13. Chan, W. and Steger, J., "A Generalized Scheme for Three-Dimensional Hyperbolic Grid Generation," AIAA paper, 91-1588, June, 1991.
14. Gill, P., Murray, W., Saunders, M., and Wright, M., "User's Guide for NPSOL: A Fortran Package for Nonlinear Programming," Tech. Report SOL 86-2, Dept. of Operations Research, Stanford University, 1986.